

# Learning the Dynamics of a Unified Quadrupedal Model

Jiayu Ding

## I. INTRODUCTION

Legged locomotion has become an increasingly prominent area of research, as it has applications in biomechanics, robotics, and evolutionary biology. By studying how animals move, researchers can gain insight into the motion patterns of animals and develop better mobile robots. There has been considerable interest in the studies of the periodic motion patterns of legged systems, also known as *gaits*. These gaits have been found to have a number of distinct properties depending on the terrain, speed and size of the organism. It has been hypothesized that gaits play a key role in maintaining balance and stability, as well as saving energy by enabling animals to move in a more efficient manner at various speeds [1]. Pioneers such as Milton Hildebrand and Robert McNeill Alexander studied the locomotion of hundreds of quadrupedal vertebrates and discovered that these animals use a large variety of gaits depending upon their species and morphology [2], [3]. However, learning the dynamics of animal locomotion can be challenging due to the complexity of muscle-skeleton systems and the involvement of soft tissues.

The center of mass dynamics and kinematics for a wide variety of cursorial animals can be modeled using a simplified “template” approach with minimal degrees of freedom [4]. [5] demonstrated that an Inverted Pendulum model (IP) with two rigid legs is capable of walking on a sloped ramp without the help of any additional controllers or actuators. A Spring-Loaded Inverted Pendulum (SLIP) model explains the kinetic and potential energy exchanges in running gaits [6], [7]. These models have been shown to explain the locomotion of cursorial animals that differ greatly in size, leg number, or posture. The simplicity and broad applicability of these template models have made them invaluable for designing controllers for legged robots [8], [9].

Although these simplified models have been useful for generating single-gait controllers, efficient and reliable transitioning between gaits has been a consistent challenge for legged robotics. Many robots use a heuristic controller that initiates a gait transition by either stopping locomotion entirely and then performing a sequence of procedures to guide the system into another gait pattern or adding energy into the system by providing a thrust during the stance phases. These existing controllers usually generate abrupt changes in center of mass trajectories or leg speeds [10], [11]. Most recently, reinforced learning controllers [12], [13] have been proposed to enable smooth and stable gait changes. However, this approach not only requires a large amount of data gathered from a particular application but very limited

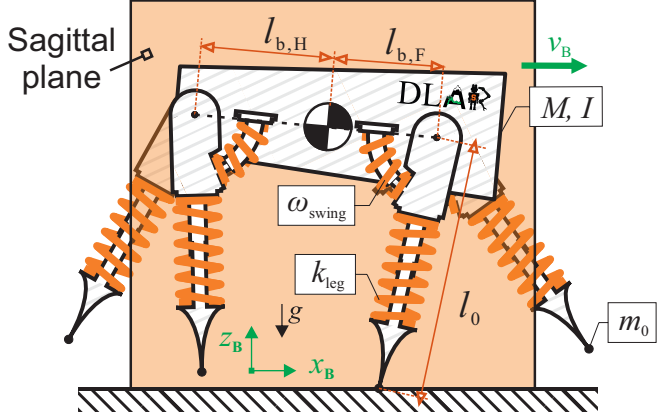


Fig. 1. A simplistic spring-mass model.

knowledge can be learned about why and how this type of controller might outperform its conventional counterparts.

To reduce the amount of training data and human efforts required to design a controller that can potentially handle various motion patterns, we expect a single model that can reproduce numerous motion patterns with the minimum computational resource cost. For bipedal locomotion, [14] found that a unified SLIP model can explain both bipedal walking and running gaits, which suggests that these two gaits are different oscillation modes of the same mechanical system with different energy levels. Similar studies for quadrupedal locomotion showed that a template SLIP model was able to reproduce horse walking, trotting and tolting gaits [15], [16]. However, the dynamics of such models will hugely rely on the system parameters like the angles of attacks and system energy, which may exponentially increase the computational efforts for solution searching of such systems.

One simple solution for the issue is to include the swing motion of the legs into the passive dynamics of the system, which has been shown on a bipedal model that is able to reproduce all common bipedal gaits [17]. For the following of this research, we built upon previous templates to provide the first unified model that is able to reproduce all common quadrupedal gaits while including the swing leg motions as part of the system dynamics.

## II. METHODS

### A. Model Description

The quadrupedal model used in this study consists of an extended main body with mass  $M$  and inertia  $J$  (Fig. 1a). The vertical and horizontal positions of the COM of the main body and the main body’s pitch angle were given by the variables  $x$ ,  $y$ , and  $\phi$ , respectively. Each pair of legs (with

index  $i \in [H, F]$ ) was modeled as a massless linear spring with length  $l_i$ , rest leg length  $l_o$ , total spring stiffness  $k_{\text{leg}}$ , no damping, and a point mass  $m$  at the foot. The leg pairs were connected to the main body through frictionless rotational joints with joint angle  $\alpha_i$ . The hip joint (back leg pair) was located at a distance of  $l_{b,H}$  behind the COM of the main body and the shoulder joint at a distance of  $l_{b,F}$  in front of the COM. We defined the value of  $l_{b,H}$  to have a negative sign. Torsional springs with stiffness  $k_{\text{swing}}$  and no damping were added to these joints. The springs are uncompressed at zero leg angles when the main body and the respective leg are perpendicular to each other. Rather than defining a value for  $k_{\text{swing}}$  directly, we prescribed a leg swing frequency  $\omega_{\text{swing}}$ , and derive:

$$k_{\text{swing}} = \omega_{\text{swing}}^2 m l_o^2. \quad (1)$$

While this model is energetically conservative during flight, it would lose energy when a foot's velocity is brought to zero in a touch-down collision. With such losses, it would be impossible to identify passive periodic gaits. To resolve this issue, we took the limit of  $m$  going towards zero ( $m \rightarrow 0$ ), similar to the method used in [18] and [19]. This implies that  $k_{\text{swing}} \rightarrow 0$  as the swing frequency  $\omega_{\text{swing}}$  remains unchanged. During the swing, dynamics along the legs are ignored, and the leg length remains as a constant value of their uncompressed length  $l_o$ . To focus on the dynamics of the proposed model, we assume the ground to be flat and rigid and that there is no foot slipping during the stance phase.

### B. Equations of Motion

We define the states of the system using the positions and pitching angle of the torso, and the relative angle between front/hind legs and the torso. The system state vector can then be written as  $\mathbf{q} := [x, y, \phi, \alpha_F, \alpha_H]^T$ , with the configuration space  $\mathbf{q} \in \mathcal{R}^2 \times \mathcal{S}^3$ . The system parameters are described: mass of the torso and the foot  $M$  and  $m$ , inertia of the torso  $J$ , center of Mass (CoM) location  $l_b$ , length of the torso and the leg  $L$  and  $l$ , torsional spring stiffness  $k_{\text{swing}}$ , and gravity  $g$ .

By applying the Euler-Lagrange equation, the equations of motion of a legged robot can be expressed in the following form:

$$\mathbf{M}(\mathbf{q})\ddot{\mathbf{q}} + \mathbf{C}(\mathbf{q}, \dot{\mathbf{q}})\dot{\mathbf{q}} + \mathbf{G}(\mathbf{q}) = \mathbf{S}\boldsymbol{\tau} + \mathbf{J}^\top(\mathbf{q})\boldsymbol{\lambda}. \quad (2)$$

where  $\mathbf{M}(\mathbf{q})$  is the inertia matrix;  $\mathbf{C}(\mathbf{q}, \dot{\mathbf{q}})$  is the Coriolis matrix; and  $\mathbf{G}(\mathbf{q})$  is the gravitational vector.  $\boldsymbol{\tau}$  denotes the vector of joint motor torques and  $\mathbf{S}$  is the selection matrix that assigns motor torques to the generalized coordinates. When a leg is in stance, the resulting ground reaction force  $\boldsymbol{\lambda}$  is mapped to the joints through Jacobi mapping  $\mathbf{J}^\top(\mathbf{q})$ .

The system dynamics naturally divide into two parts: the swing phase dynamics and the stance phase dynamics. Here, we showcase an example of each case instead of showing the overall EOMs for the hybrid system.

During the swing phase, the leg length is set to  $l_i = l_o$ , and the leg angle accelerations are given by:

$$\ddot{\alpha}_i = -\ddot{\phi} - 1/l_o \left( \cos(\alpha_i + \phi) \ddot{x} + \sin(\alpha_i + \phi) (g + \ddot{y}) \right. \\ \left. - l_b \sin(\alpha_i) \ddot{\phi} + l_b \cos(\alpha_i) \dot{\phi}^2 + 1/l_o k_{\text{swing}} \alpha_i \right). \quad (3)$$

, where the detailed derivative of the EOMs is included in Appendix A.

During the stance phase, the equations of motion (EOM) are given for the main body:

$$\ddot{x} = F_x/M, \quad \ddot{y} = F_y/M - g, \quad \ddot{\phi} = \tau/J, \quad (4)$$

where  $F_x$ ,  $F_y$ , and  $\tau$  are the net forces and torques created by the leg pairs. Depending on whether the leg pairs are in the air or in contact with the ground, their dynamics differ. During stance, the leg angle and leg length are computed from kinematic constraints, as we assume no sliding of the foot. The leg length is given by  $l_i = \frac{y + l_b \sin(\phi)}{\cos(\alpha_i + \phi)}$ , and the leg angle follows from

$$x + l_b \cos(\phi) + \tan(\alpha_i + \phi) (y + l_b \sin(\phi)) = x_{foot,i}, \quad (5)$$

where  $x_{foot,i}$  is the horizontal position of the foot on the ground. We solved this equation explicitly for leg velocities and accelerations, allowing us to express the leg angle in both the stance and swing phase as a second-order differential equation, where the detailed derivative of the EOMs is included in Appendix A.

### C. Footfall Sequence

In order to determine the footfall pattern of a stride, we introduced four timing variables  $t_j$ , ( $j \in [Htd, Hlo, Ftd, Flo]$ ) for the touch-down and lift-off events. To enable solutions with different footfall patterns, the order of these events can be arbitrary, but their values are confined within the time interval of one stride  $[0, t_{\text{stride}}]$ . These timing variables are used to determine whether a leg pair is in the air or on the ground at a given time  $t$ . The timing vector  $\mathbf{e}^T = [t_{Htd}, t_{Hlo}, t_{Ftd}, t_{Flo}]$  thus breaks the whole stride into 5 distinct intervals, each next interval with a different contact configuration. Using the position and velocity vector  $\mathbf{q}^T := [x, y, \phi, \alpha_F, \alpha_H]$ ,  $\dot{\mathbf{q}}^T := [\dot{x}, \dot{y}, \dot{\phi}, \dot{\alpha}_F, \dot{\alpha}_H]$  to describe the state of the system, we express the dynamics as a time variant differential equation  $\ddot{\mathbf{q}} = f(\mathbf{q}, \dot{\mathbf{q}}, t, \mathbf{e})$  which is parameterized by  $\mathbf{e}$ . In addition, at the moments of touch-down  $t_k$ , ( $k \in [Htd, Ftd]$ ), we need to reset the leg velocities according to the derivative of equation (5) resulting in the additional discrete dynamics  $\dot{\mathbf{q}}(t_k^+) = h(\mathbf{q}(t_k^-), \dot{\mathbf{q}}(t_k^-))$ .

### D. Gait Creation

We defined a gait as a periodic motion in which all states except for the horizontal position  $x$  return to their original values after one full *stride*. Without loss of generality, the apex transition ( $\dot{y} = 0$ ) was selected as the Poincaré section

for this limit cycle analysis. Finding a gait in this model was thus equivalent to solving the following problem:

$$\mathbf{T}(\mathbf{Z}^*) := \begin{bmatrix} \ddot{\mathbf{q}} - \mathbf{f}(\mathbf{q}, \dot{\mathbf{q}}, t, \mathbf{e}) \\ \dot{\mathbf{q}}(t_k^+) - h(\mathbf{q}(t_k^-), \dot{\mathbf{q}}(t_k^-)) \\ R_{1-14}(\mathbf{q}, \dot{\mathbf{q}}, \mathbf{e}, t_{\text{stride}}) \end{bmatrix} = \mathbf{0}. \quad (6)$$

The solution vector of this equation,  $\mathbf{Z}^* := (\mathbf{q}, \dot{\mathbf{q}}, \mathbf{e}, t_{\text{stride}})$ , combines the generalized positions and velocities of the model ( $\mathbf{q}$  and  $\dot{\mathbf{q}}$ ) with the vector of footfall timings  $\mathbf{e}$  and the overall stride time  $t_{\text{stride}}$ . The boundary and interior-point conditions in  $R_{1-14}$  were used to enforce (I) that all positions except  $x$  are periodic ( $R_{1-4}$ ), (II) that all velocities are periodic ( $R_{5-9}$ ), (III) that the stride ends at the Poincaré section ( $R_{10}$ ), and (IV) that the legs are fully extended at touchdown and liftoff ( $R_{11-14}$ ):

$$\begin{aligned} R_{1-4} &= \bar{\mathbf{q}}(t_{\text{stride}}) - \bar{\mathbf{q}}(t=0), \\ R_{5-9} &= \dot{\mathbf{q}}(t_{\text{stride}}) - \dot{\mathbf{q}}(t=0), \\ R_{10} &= \dot{y}(t_{\text{stride}}), \\ R_{11-14} &= y(t_j) + l_{b,i} \sin(\phi(t_j)) \\ &\quad - l_o \cos(\phi(t_j) + \alpha_i(t_j)). \end{aligned} \quad (7)$$

### E. Continuation and Bifurcations

We found all solutions of eq. (6) through numerical continuation and bifurcation analysis, similar to the continuation approach presented in [?]. That is, starting from an initial solution  $\mathbf{Z}_1$ , we computed branches of solutions iteratively. Assuming that  $\mathbf{Z}_n^*$  is the  $n^{\text{th}}$  solution that we found, we numerically search for an adjacent solution  $\mathbf{Z}_{n+1}^*$  in a two-step predictor-corrector process (Fig. 2): first we determine an initial guess  $\mathbf{Z}_{n+1}^o = \mathbf{Z}_n^* + d \cdot (\mathbf{Z}_n^* - \mathbf{Z}_{n-1}^*)$ , by continuing to move with a fixed step length of  $d$  tangentially along the existing solution branch. We then identify the exact solution  $\mathbf{Z}_{n+1}^*$  by numerically solving the following constrained problem:

$$\mathbf{T}(\mathbf{Z}_{n+1}^*) = \mathbf{0}, \quad (8a)$$

$$\|\mathbf{Z}_{n+1}^* - \mathbf{Z}_n^*\| = d, \quad (8b)$$

$$(\mathbf{Z}_{n+1}^* - \mathbf{Z}_n^*)^T (\mathbf{Z}_n^* - \mathbf{Z}_{n-1}^*) > 0. \quad (8c)$$

Here, eq. (8a) ensures that the new solution fulfills (6), eq. (8b) ensures that we move with a constant step length along the branch, and eq. (8c) ensures that we are not stepping backwards. By iteratively repeating these two steps, we can identify complete solution branches.

## III. RESULTS

This section showcases our primary discoveries and illustrates how different parameter bifurcations break symmetries in a simplistic model in distinct ways, leading to various quadrupedal gaits and footfall patterns. In particular, we employed numerical continuation techniques outlined in our earlier research [17] and sought out periodic solutions for the model defined in equation (??). In this study, we revealed four unique quadrupedal gaits (pronking, bounding, half-bounding, and galloping) that demonstrate interconnections

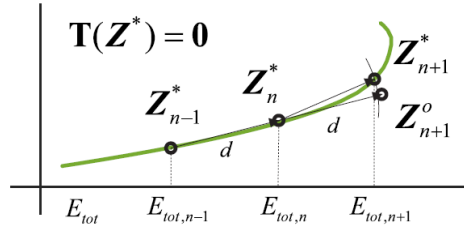


Fig. 2. The continuation algorithm used in this work employs a prediction-correction process. We first determine an initial guess  $\mathbf{Z}_{n+1}^o$  of a new solution by moving tangentially along the branch with a step length of  $d$ . We then numerically solve eq. (8) to find an exact new solution  $\mathbf{Z}_{n+1}^*$ .

through diverse parameter bifurcations. The naming conventions of several common quadrupedal gaits were adopted from the animal locomotion literature using the footfall patterns [2], [20]. In order to generalize our results for systems with different sizes, we normalized all the values in our results using total mass  $m$  of the entire system, resting leg length  $l_o$ , and gravity  $g$ . In order to have an energy-conservative system and avoid collision losses, we took the limit of the foot mass  $m_o$  to zero so that  $m = M + 4m_o = M$ . In addition, we took the limit of the foot mass  $m_o$  to zero so that  $m = M + 4m_o = M$  to have an energy-conservative system and avoid collision losses. For simplicity, most of the system parameters were fixed in this study with  $k_{\text{leg}} = 10$  [ $mg/l_o$ ],  $\omega_{\text{swing}} = 20$  [ $\sqrt{g/l_o}$ ], and  $I = 2$  [ $ml_o^2$ ] according to the values used by animals as described in [21]–[23].

To better understand the symmetry-breaking process, we started the search with a quadrupedal model characterized by the largest set of morphological symmetries *i.e.*, all four legs were identical and the COM was at the geometric center of the torso. Then we broke various types of symmetries described in the method section by varying the total energy  $E(\mathbf{q}, \dot{\mathbf{q}})$  stored in the system and the COM location  $l_b$  of the torso and analyzed their influences on the footfall patterns of periodic gaits. To simplify the numerical calculations and the analysis of the periodic orbits, we selected the apex transition in the flight phase as the Poincaré section  $\mathcal{P} = \{(\mathbf{q}, \dot{\mathbf{q}}) \in \mathcal{T}\mathcal{Q} \mid \dot{q}_z = 0, \dot{q}_z < 0, (t_i^{\text{TD}}(\mathbf{q}, \dot{\mathbf{q}}) \bmod T) < (t_i^{\text{LO}}(\mathbf{q}, \dot{\mathbf{q}}) \bmod T)\}$ . In the following figures, the fixed points  $\mathcal{P}^* := \mathcal{P}(t) = \mathcal{P}(t+T)$  on the Poincaré section *i.e.*, the periodic orbits  $\mathcal{O}$  are visualized using the torso's horizontal velocity  $\dot{q}_x$  and pitching velocity  $\dot{q}_{\text{pitch}}$ .

### A. Pronking and Bounding Gaits

1) *Pronking* (PF): is a quadrupedal gait frequently observed in quadrupedal animals, characterized by the synchronized movement of all four legs. During a single stride, there is only one flight phase followed by a stance phase, during which all four legs make contact with the ground, moving in precisely the same manner. This results in zero torque on the torso and the torso has no rotational motion throughout the stride ( $\dot{q}_{\text{pitch}} = 0$  [ $\text{rad}/\text{s}$ ]). Our parameter continuation process initiated with a simple seed solution, where the model executed an in-place jump, with all four legs aligned

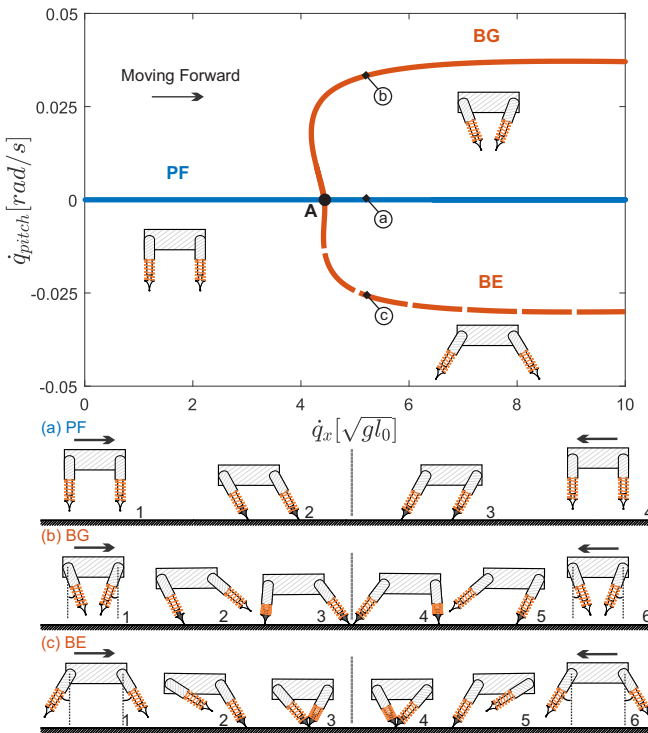


Fig. 3. Gait branches of pronking forward (PF), bounding with gathered suspension (BG), and bounding with extended suspension (BE) on the Poincare section with the torso's horizontal velocity  $\dot{q}_x$  as the horizontal axis and pitching velocity  $\dot{q}_{pitch}$  as the vertical axis. Examples of each gait (a-c) are shown as successive keyframes at the touch-down, lift-off moments, and the apex at the bottom. Black feet are used to highlight the legs in stance.

vertically downward ( $\dot{q}_x = 0 [\sqrt{gl_o}]$  and  $\dot{q}_{pitch} = 0 [rad/s]$ ). When the overall energy in the system was modified, the resulting solutions constituted a one-dimensional curve (blue curve in Fig. 3) with varying average speeds. Multiple consecutive keyframes of the pronking gait, starting with an initial speed of  $5.2 [\sqrt{gl_o}]$ , at the instances of the apex, touchdown, and liftoff, were illustrated in Figure 3(a).

2) *Bounding* (BG and BE): Compared to pronking gaits, bounding gaits exhibit a breakdown in the coordination between the front and hind legs. Despite the synchronized movements within the front and hind leg pairs, there is a phase delay between legs on the same sides, leading to two touchdown and liftoff events within a single stride. Our model yielded two distinct types of solutions that adhere to this pattern. In the first type of bounding gait, as depicted in Fig. 3(b), the hind leg pair makes initial contact with the ground, followed by the front legs, causing the leg pairs to converge inward during the flight phase. This particular gait is referred to as *bounding with gathered suspension*, as described in [24], and we'll abbreviate it as BG hereafter. In Fig. 3, these solutions are represented by the solid orange curve, which bifurcates from the PF branch at  $\dot{q}_x = 4.4 [\sqrt{gl_o}]$  (designated as black dot A). The other type of bounding gait is characterized by the opposite sequence of touch-downs, as shown in Fig. 3(c), where the front legs touch the ground first, followed by the hind legs. Consequently, the swing leg pairs extend outward during the flight phase, termed *bounding with extended suspension*

(BE). In Fig. 3, these solutions are represented by red dashed curves, connected to the pronking branch at the same bifurcation point A.

### B. Half-Bounding and Galloping Gaits

1) *Half-Bounding* (FG, FE, HG, and HE): are similar to bounding gaits but the synchronization is broken in one leg pair. In these gaits, one of the leg pairs makes contact with the ground simultaneously, while the other leg pair touches down in rapid succession. Consequently, half-bounding gaits can be classified as 3-beat gaits. We found in total four variations of them based on the footfall patterns as shown in Fig. 4. When this desynchronization occurred in the hind leg pair, we found “half-bounding with spread Hind legs and Gathered suspension” (HG) and “half-bounding with spread Hind legs and Extended suspension” (HE). Similar to the distinction between bounding gaits in BG and BE branches, solutions within the FG and FE branches exhibit varying leg orientations and pitching velocities during the apex transitions. For instance, as depicted in Fig. 4, the HG gait branch (yellow solid curve) emerges from point B on BG at a speed of  $\dot{q}_x = 4.6 [\sqrt{gl_o}]$ , while the HE branch (yellow dashed curve) originates at point C on BE with a speed of  $\dot{q}_x = 6.1 [\sqrt{gl_o}]$ . As the solutions along the HG and HE branches approach point A, all four legs tend to synchronize, ultimately converging with the pronking branch at point A. The keyframes of periodic solutions for these two gaits at the moments of touchdown, liftoff, and the apex transition are illustrated in Fig. 4(f)&(h). On the other hand, when the symmetry breaking occurred in the front leg pair, we identified two additional half-bounding gaits characterized by front legs in a spread position and gathered suspension (FG) and front legs in a spread position and extended suspension (FE). These two branches are represented as green solid/dashed curves in Fig. 4, and they connect to the bounding gaits BG and BE at bifurcation points D and E, respectively, with forward speeds of  $5.7 [\sqrt{gl_o}]$  and  $4.8 [\sqrt{gl_o}]$ , correspondingly. Similarly, the FG and FE branches ultimately converge with the pronking branch and merge at bifurcation point A. Keyframes illustrating these two gait solutions can be observed in Fig. 4(g)&(i).

2) *Galloping*: In the study conducted by Hilderbrand (1989) [25], a range of galloping gaits was identified, each characterized by unique footfall patterns and aerial suspension. In our research, we analyzed galloping patterns from the proposed model and discovered two distinct types: “galloping with gathered suspension” (GG) and “galloping with extended suspension” (GE). These patterns are represented by purple curves in Fig. 5, connecting to the FG and HE branches at bifurcation points F and G, marked as stars, with speeds of  $\dot{x} = 6.0 [\sqrt{gl_o}]$  and  $\dot{x} = 6.2 [\sqrt{gl_o}]$  respectively. Similar to the bounding gaits, these galloping gaits exhibit unique touchdown sequences and swinging leg motions, reminiscent of the galloping movements observed in natural horses and gazelles.

#### IV. CONCLUSIONS AND FUTURE WORKS

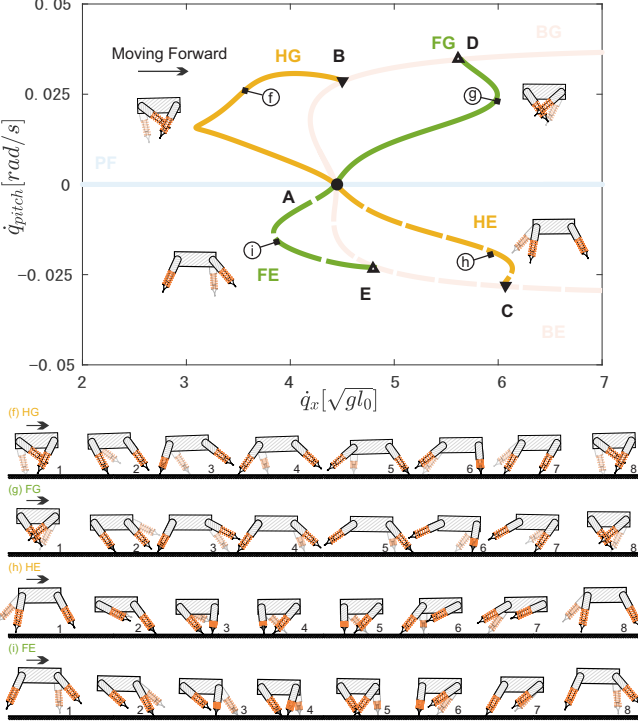


Fig. 4. This figure illustrates the gait branches of half-bounding as identified from the proposed model. Since symmetry breaking can occur in either the front or hind leg pair, during the numerical search, a total of four such gait patterns were discovered from the two bounding gaits (BG and BE): (f) and (g) demonstrate half-bounding gaits with gathered suspensions; (h) and (i) illustrate half-bounding gaits with extended suspensions.

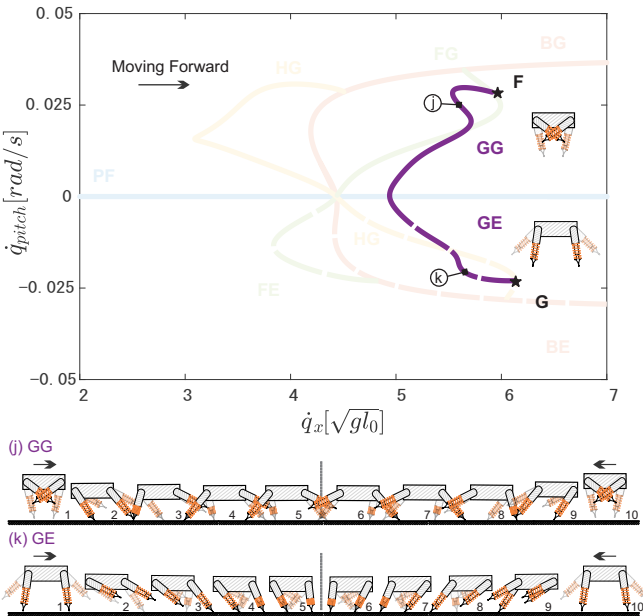


Fig. 5. This figure displays the solution branch and keyframes for two galloping gaits: (j) Galloping with gathered suspension (GG); (k) Galloping with extended suspension (GE). In this visualization, the left legs are presented in a transparent color, while black feet are employed to emphasize the legs in the stance phase.

In this work, we systematically investigated the dynamics of a unified model, an extended version of the SLIP model that reproduces all common quadrupedal gaits. The system involves hybrid dynamics, which consist of swing and stance dynamics and their transitions. The contact phases determine the EOMs. We tested the model's dynamics by running numerical simulations using MATLAB and introduced our preliminary results by showing four types of gaits: pronking, bounding, half-bounding, and galloping. The gaits are related through bifurcations by breaking symmetries in the solutions. However, since the event timings, which are time-dependent system parameters, are included as part of the solution for the current framework, we are not able to precisely identify the bifurcation points by showing the local Floquet analysis.

Future work will mainly focus on addressing the bifurcation identification problem. While there exists research that introduces local Floquet analysis with system parameters involved, a more promising way of doing this will be similar to including the swing leg motions into the system dynamics, which is to eliminate the role of timing parameters in simulation by introducing extra states of the system, e.g., by introducing leg length as addition states, the framework may be able to transition between swing and stance phase whenever the return map is triggered by the leg length constraints.

#### REFERENCES

- [1] D. F. Hoyt and C. R. Taylor, "Gait and the energetics of locomotion in horses," *Nature*, vol. 292, no. 5820, pp. 239–240, July 1981. [Online]. Available: <https://doi.org/10.1038/292239a0>
- [2] M. Hildebrand, "Symmetrical gaits of horses," *Science*, vol. 150, no. 3697, pp. 701–708, Nov. 1965. [Online]. Available: <https://doi.org/10.1126/science.150.3697.701>
- [3] R. M. Alexander, *Principles of Animal Locomotion*. Princeton University Press, Jan. 2002. [Online]. Available: <https://doi.org/10.1515/9781400849512>
- [4] R. Full and D. Koditschek, "Templates and anchors: neuromechanical hypotheses of legged locomotion on land," *Journal of Experimental Biology*, vol. 202, no. 23, pp. 3325–3332, Dec. 1999. [Online]. Available: <https://doi.org/10.1242/jeb.202.23.3325>
- [5] T. McGeer, "Passive dynamic walking," *The International Journal of Robotics Research*, vol. 9, no. 2, pp. 62–82, Apr. 1990. [Online]. Available: <https://doi.org/10.1177/027836499000900206>
- [6] R. Blickhan, "The spring-mass model for running and hopping," *Journal of Biomechanics*, vol. 22, no. 11-12, pp. 1217–1227, Jan. 1989. [Online]. Available: [https://doi.org/10.1016/0021-9290\(89\)90224-8](https://doi.org/10.1016/0021-9290(89)90224-8)
- [7] C. T. Farley, J. Glasheen, and T. A. McMahon, "Running springs: speed and animal size," *Journal of Experimental Biology*, vol. 185, no. 1, pp. 71–86, Dec. 1993. [Online]. Available: <https://doi.org/10.1242/jeb.185.1.71>
- [8] S. Rezazadeh, C. Hubicki, M. Jones, A. Peekema, J. Van Why, A. Abate, and J. Hurst, "Spring-mass walking with atrias in 3d: Robust gait control spanning zero to 4.3 kph on a heavily underactuated bipedal robot," in *Dynamic Systems and Control Conference*, vol. 57243. American Society of Mechanical Engineers, 2015, p. V001T04A003.
- [9] A. Hereid, S. Kolathaya, M. S. Jones, J. V. Why, J. W. Hurst, and A. D. Ames, "Dynamic multi-domain bipedal walking with atrias through SLIP based human-inspired control," in *Proceedings of the 17th international conference on Hybrid systems: computation and control*. ACM, Apr. 2014. [Online]. Available: <https://doi.org/10.1145/2562059.2562143>

- [10] D. J. Hyun, S. Seok, J. Lee, and S. Kim, "High speed trot-running: Implementation of a hierarchical controller using proprioceptive impedance control on the mit cheetah," *The International Journal of Robotics Research*, vol. 33, no. 11, pp. 1417–1445, 2014.
- [11] D. J. Hyun, J. Lee, S. Park, and S. Kim, "Implementation of trot-to-gallop transition and subsequent gallop on the mit cheetah i," *The International Journal of Robotics Research*, vol. 35, no. 13, pp. 1627–1650, 2016.
- [12] J. Hwangbo, J. Lee, A. Dosovitskiy, D. Bellicoso, V. Tsounis, V. Koltun, and M. Hutter, "Learning agile and dynamic motor skills for legged robots," *Science Robotics*, vol. 4, no. 26, 2019.
- [13] J. Siekmann, Y. Godse, A. Fern, and J. Hurst, "Sim-to-real learning of all common bipedal gaits via periodic reward composition," *arXiv preprint arXiv:2011.01387*, 2020.
- [14] H. Geyer, A. Seyfarth, and R. Blickhan, "Compliant leg behaviour explains basic dynamics of walking and running," *Proceedings of the Royal Society B: Biological Sciences*, vol. 273, no. 1603, pp. 2861–2867, Aug. 2006. [Online]. Available: <https://doi.org/10.1098/rspb.2006.3637>
- [15] Z. Gan and C. D. Remy, "A passive dynamic quadruped that moves in a large variety of gaits," in *Intelligent Robots and Systems (IROS 2014), 2014 IEEE/RSJ International Conference on*. IEEE, 2014, pp. 4876–4881.
- [16] Z. Gan, T. Wiestner, M. A. Weishaupt, N. M. Waldern, and C. D. Remy, "Passive dynamics explain quadrupedal walking, trotting, and tölting," *Journal of computational and nonlinear dynamics*, vol. 11, no. 2, p. 021008, 2016.
- [17] Z. Gan, Y. Yesilevskiy, P. Zaytsev, and C. D. Remy, "All common bipedal gaits emerge from a single passive model," *Journal of The Royal Society Interface*, vol. 15, no. 146, p. 20180455, Sept. 2018. [Online]. Available: <https://doi.org/10.1098/rsif.2018.0455>
- [18] M. Garcia, A. Chatterjee, A. Ruina, and M. Coleman, "The simplest walking model: stability, complexity, and scaling," *J Biomech Eng Trans ASME*, vol. 120, no. 2, pp. 281–288, 1998.
- [19] S. M. O'Connor, "The relative roles of dynamics and control in bipedal locomotion," Ph.D. dissertation, University of Michigan, 2009.
- [20] R. M. Alexander, "The gaits of bipedal and quadrupedal animals," *The International Journal of Robotics Research*, vol. 3, no. 2, pp. 49–59, June 1984. [Online]. Available: <https://doi.org/10.1177/027836498400300205>
- [21] R. Blickhan and R. Full, "Similarity in multilegged locomotion: Bouncing like a monopode," *Journal of Comparative Physiology A*, vol. 173, no. 5, Nov. 1993. [Online]. Available: <https://doi.org/10.1007/bf00197760>
- [22] D. T. Polet, "The murphy number: how pitch moment of inertia dictates quadrupedal walking and running energetics," *Journal of Experimental Biology*, vol. 224, no. 5, Mar. 2021. [Online]. Available: <https://doi.org/10.1242/jeb.228296>
- [23] J. Ding, T. Y. Moore, and Z. Gan, "A template model explains jerboa gait transitions across a broad range of speeds," *Frontiers in Bioengineering and Biotechnology*, vol. 10, Apr. 2022. [Online]. Available: <https://doi.org/10.3389/fbioe.2022.804826>
- [24] M. Hildebrand, "Analysis of asymmetrical gaits," *Journal of Mammalogy*, vol. 58, no. 2, pp. 131–156, May 1977. [Online]. Available: <https://doi.org/10.2307/1379571>
- [25] ———, "The quadrupedal gaits of vertebrates," *BioScience*, vol. 39, no. 11, pp. 766–775, Dec. 1989. [Online]. Available: <https://doi.org/10.2307/1311182>

## APPENDIX A DETAILED DERIVATIVE OF THE EOMs

We define the states of the system using the positions and pitching angle of the torso, and the relative angle between front/hind legs and the torso. The system state vector can then be written as:

$$\mathbf{q} := [x, y, \phi, \alpha_F, \alpha_H]^T, \text{ and, } \dot{\mathbf{q}} := [\dot{x}, \dot{y}, \dot{\phi}, \dot{\alpha}_F, \dot{\alpha}_H]^T$$

with the configuration space  $\mathbf{q} \in \mathcal{R}^2 \times \mathcal{S}^3$ . The system parameters are described: mass of the torso and the foot  $M$  and  $m$ , inertia of the torso  $J$ , center of Mass (CoM) location  $l_b$ , length of the torso and the leg  $L$  and  $l$ , torsional spring stiffness  $k_{swing}$ , and gravity  $g$ .

### A. Swing phase dynamics

In this section, we aim to derive the EOM for the swing phase using the Lagrangian method. To do so, we first express the positions of the front and hind foot using generalized coordinates  $\mathbf{q}$ :

$$\begin{aligned} pos_{FFoot} &= pos_F + l \begin{bmatrix} \sin(\alpha_F + \phi + \pi) \\ -\cos(\alpha_F + \phi + \pi) \end{bmatrix}, \quad pos_F = pos_0 + (1 - l_b) \cdot L \cdot \begin{bmatrix} \cos(\phi + \pi) \\ \sin(\phi + \pi) \end{bmatrix} \\ pos_{HFoot} &= pos_H + l \begin{bmatrix} \sin(\alpha_H + \phi) \\ -\cos(\alpha_H + \phi) \end{bmatrix}, \quad pos_H = pos_0 + l_b \cdot L \cdot \begin{bmatrix} \cos(\phi) \\ \sin(\phi) \end{bmatrix} \end{aligned}$$

where  $pos_0 = [x, y]^T$ .

The Jacobian matrix  $J_{S0}$  for the position of the CoM with respect to the state variables  $q = [x, y, \phi, \alpha_H, \alpha_F]$  is:

$$J_{S0} = \frac{\partial pos_0}{\partial q} = \begin{bmatrix} 1 & 0 & 0 & 0 & 0 \\ 0 & 1 & 0 & 0 & 0 \end{bmatrix}$$

and the rotational Jacobian  $J_{R0}$  for the pitching angle  $\phi$ , which affects only the rotational components, is:

$$J_{R0} = \frac{\partial \phi}{\partial q} = \begin{bmatrix} 0 & 0 & 1 & 0 & 0 \end{bmatrix}$$

Given the dependencies of  $pos_{FFoot}$  on the configuration variables, the Jacobian  $J_{SFF}$  can be represented as:

$$J_{SFF} = \begin{bmatrix} 1 & 0 & (1 - l_b)L \sin(\phi + \pi) + l \cos(\alpha_F + \phi + \pi) & 0 & l \cos(\alpha_F + \phi + \pi) \\ 0 & 1 & -(1 - l_b)L \cos(\phi + \pi) - l \sin(\alpha_F + \phi + \pi) & 0 & l \sin(\alpha_F + \phi + \pi) \end{bmatrix}$$

and for the  $pos_{HFoot}$ , given its dependencies, the Jacobian  $J_{SHF}$  is:

$$J_{SHF} = \begin{bmatrix} 1 & 0 & l_b L \sin(\phi) + l \cos(\alpha_H + \phi) & l \cos(\alpha_H + \phi) & 0 \\ 0 & 1 & -l_b L \cos(\phi) - l \sin(\alpha_H + \phi) & l \sin(\alpha_H + \phi) & 0 \end{bmatrix}$$

We now derive the kinetic energy of the system, which includes the rotational kinetic energy of the torso along with the translational kinetic energy of the torso and limbs. We have:

$$\begin{aligned} T_{\text{CoM,trans}} &= \frac{1}{2} M ((J_{S0} \cdot \dot{\mathbf{q}})^T \cdot (J_{S0} \cdot \dot{\mathbf{q}})) \\ T_{\text{CoM,rot}} &= \frac{1}{2} J ((J_{R0} \cdot \dot{\mathbf{q}})^T \cdot (J_{R0} \cdot \dot{\mathbf{q}})) \end{aligned}$$

for the torso and

$$T_{\text{limbs}} = \frac{1}{2} m ((J_{SFF} \cdot \dot{\mathbf{q}})^T \cdot (J_{SFF} \cdot \dot{\mathbf{q}}) + (J_{SHF} \cdot \dot{\mathbf{q}})^T \cdot (J_{SHF} \cdot \dot{\mathbf{q}}))$$

for the limbs. The total kinetic energy  $T$  is:

$$T = T_{\text{CoM,trans}} + T_{\text{CoM,rot}} + T_{\text{limbs}}$$

Due to the page limit, the detailed kinetic energy expression cannot be shown in the manuscript. We include the MATLAB code to derive the kinetic energy of the system, as well as the whole EOMs in the following link <https://github.com/JY-Din/MEE725-Term-Paper-Spring2024.git>. The potential energy, primarily due to gravity, remains as previously defined but reiterated here for completeness:

$$V = (M + 2m)gy + mgl_0(\sin(\alpha_F + \phi) + \sin(\alpha_H + \phi))$$

Given the Lagrangian  $L$  of the system as the difference between the kinetic energy  $T$  and the potential energy  $V$ :

$$L = T - V$$

We can derive the EOMs using Euler-Lagrange equation:

$$\frac{d}{dt} \left( \frac{\partial L}{\partial \dot{q}_i} \right) - \frac{\partial L}{\partial q_i} = 0$$

where  $q_i$  represents each generalized coordinate  $x, y, \phi, \alpha_F, \alpha_H$ . The mentioned calculation can be easily delivered by taking the Jacobian of the Lagrangian  $L$  with respect to  $\mathbf{q}$  and  $\dot{\mathbf{q}}$ :

$$\frac{dL}{d\mathbf{q}} = \text{Jacobian}(L, \dot{\mathbf{q}}), \quad \frac{dL}{d\dot{\mathbf{q}}} = \text{Jacobian}(L, \mathbf{q}), \quad \frac{d}{dt} \left( \frac{dL}{d\dot{\mathbf{q}}} \right) = \text{Jacobian} \left( \frac{dL}{d\dot{\mathbf{q}}}, \mathbf{q} \right) \cdot \dot{\mathbf{q}}$$

We can then acquire the mass matrix and the Coriolis and gravitational forces as:

$$M = \text{Jacobian} \left( \frac{dL}{d\dot{\mathbf{q}}}, \dot{\mathbf{q}} \right), \quad f_{cg} = \frac{dL}{d\mathbf{q}} - \frac{d}{dt} \left( \frac{dL}{d\dot{\mathbf{q}}} \right)$$

Given the external forces vector:  $\boldsymbol{\tau} = [0, 0, 0, -\alpha_H k_s m, -\alpha_F k_s m]^T$  The final EOMs can be written as:

$$\mathbf{M}(\mathbf{q})\ddot{\mathbf{q}} + f_{cg}(\mathbf{q}, \dot{\mathbf{q}})\dot{\mathbf{q}} = \boldsymbol{\tau}.$$

### B. Stance leg dynamics

Using exactly the same configuration space and parameter sets, we derive the EOMs for the stance phase. For the torso, we have:

$$\begin{aligned} \dot{x} &= \frac{F_{x,F} + F_{x,H}}{M} \\ \dot{y} &= \frac{F_{y,B} + F_{y,F} - g}{M} \\ \dot{\phi} &= -\frac{F_{y,B}(x - l_b \cos(\phi)) - F_{x,H}(y - l_b \sin(\phi)) - F_{y,F}(x - \cos(\phi)(l_b - 1)) + F_{x,F}(y - \sin(\phi)(l_b - 1))}{J} \end{aligned}$$

, where  $F_x$ ,  $F_y$ , and  $\tau$  are the net forces and torques created by the leg pairs.

The front/hind foot positions can be expressed as:

$$x_{F,foot} = x + \tan(\alpha_F + \phi)(y - \sin(\phi)(l_b - 1)) - \cos(\phi)(l_b - 1)$$

$$x_{H,foot} = x + \tan(\alpha_H + \phi)(y - l_b \sin(\phi)) - l_b \cos(\phi)$$

We can then express the velocity constraints and acceleration constraints:

$$\dot{x}_{F,foot} = \text{Jacobian}(x_{F,foot}, \mathbf{q}) \cdot \dot{\mathbf{q}} == 0, \quad \ddot{x}_{F,foot} = \text{Jacobian}(\dot{x}_{F,foot}, \mathbf{q}) \cdot \dot{\mathbf{q}} + \text{Jacobian}(\dot{x}_{F,foot}, \dot{\mathbf{q}}) \cdot \ddot{\mathbf{q}} == 0$$

$$\dot{x}_{H,foot} = \text{Jacobian}(x_{H,foot}, \mathbf{q}) \cdot \dot{\mathbf{q}} == 0, \quad \ddot{x}_{H,foot} = \text{Jacobian}(\dot{x}_{H,foot}, \mathbf{q}) \cdot \dot{\mathbf{q}} + \text{Jacobian}(\dot{x}_{H,foot}, \dot{\mathbf{q}}) \cdot \ddot{\mathbf{q}} == 0$$

which can be used to explicitly solve for the expressions of  $\ddot{\alpha}_i$  (shown in the code).